One-Center Charge Transfer Transitions in Manganites

A.S. Moskvin
Department of Theoretical Physics, Ural State University, 620083 Ekaterinburg, Russia
(Dated: October 26, 2018)

In frames of a rather conventional cluster approach, which combines the crystal field and the ligand field models we have considered different charge transfer (CT) states and O 2p-Mn 3d CT transitions in MnO_6^{9-} octahedra. The many-electron dipole transition matrix elements were calculated using the Racah algebra for the cubic point group. Simple "local" approximation allowed to calculate the relative intensity for all dipole-allowed $\pi-\pi$ and $\sigma-\sigma$ CT transitions. We present a self-consistent description of the CT bands in insulating stoichiometric $LaMn^{3+}O_3$ compound with the only Mn^{3+} valent state and idealized octahedral MnO_6^{9-} centers which allows to substantially correct the current interpretation of the optical spectra. Our analysis shows the multi-band structure of the CT optical response with the weak low-energy edge at 1.7 eV, associated with forbidden $t_{1g}(\pi)-e_g$ transition and a series of the weak and strong dipole-allowed high-energy transitions starting from 2.5 and 4.5 eV, respectively, and extending up to nearly 11 eV. The most intensive features are associated with two strong composite bands near $4.6 \div 4.7$ eV and $8 \div 9$ eV, respectively, resulting from the superposition of the dipole-allowed $\sigma-\sigma$ and $\pi-\pi$ CT transitions. These predictions are in good agreement with experimental spectra. The experimental data point to a strong overscreening of the crystal field parameter Dq in the CT states of MnO_6^{9-} centers.

I. INTRODUCTION

The discovery of the colossal magnetoresistance in doped manganites like $La_{1-x}Sr_xMnO_3$ have generated a flurry of the ideas, models and scenarios of this puzzling phenomena, many of which are being developed up to date, although the situation remains controversial. There are many thermodynamic and local microscopic quantities that cannot be explained by the conventional double-exchange model with the predominantly Mn 3d location of doped holes. In such a situation we argue a necessity to discuss all possible candidate states with different valent structure of manganese and oxygen atoms, as well as different valent states of octahedral MnO_6 centers.[1] Namely these slightly distorted octahedra are believed to be the basic units both for crystalline and electronic structure in manganites.

As for an examination of the energy spectrum and electronic structure one should emphasize an importance of different optical methods because these provide valuable information concerning the dielectric function. The nature of the low-energy optical electron-hole excitations in the insulating transition metal (3d-) oxides represents one of the most important challenging issues for these strongly correlated systems. It is now believed that the most intensive low-energy electronic excitations in insulating 3d-oxides correspond to the transfer of electrons from oxygen anion to 3d metal cation, hence these materials are charge transfer (CT) insulators. However, the more detailed assignment of these excitations remains open. All these are especially interesting because they could play a central role in multiband Hubbard models used to describe both the insulating state and the unconventional states developed under electron or hole doping.

It is now generally accepted that the ground state of the MnO_6 centers in $LaMnO_3$ corresponds to the orbital doublet ${}^5E_g$ term of the high-spin $t_{2g}^3e_g^1$ configuration. The optical conductivity spectrum of $LaMnO_3$ exhibits two broad peaks centered around 2.0 and 5.0 eV.[2,3,4,5] However, it has remained unclear just what the nature of the intensive low-energy optical electron-hole excitation peaked near 2.0 eV as well as more intensive excitations with higher energy peaked near 5.0 eV. Some authors[2,3,5] assign these both features to the dipole-allowed CT transitions like $t_{2g}^3e_g^1 - t_{2g}^3e_g^2\underline{L}$ and $t_{2g}^3e_g^1 - t_{2g}^4e_g^1\underline{L}$ ($\underline{L}$ denoting a ligand hole), respectively. However, others[4] assign the low-energy peak to the "intra-atomic" ${}^5E_g - {}^5E_g^{'}$ transition, or doubly-forbidden (parity and orbital quasimomentum) d-d-like crystal-field transition between two ${}^5E_g$-sublevels separated by a splitting due to low-symmetry crystalline field. Both interpretations being particularly qualitative suffer from many shortcomings and give rise to many questions concerning the details of the charge transfer states or expected extremely weak intensity for the d-d transitions.

Unfortunately, the main body of the optical data for manganites is obtained from reflectivity measurements, that often implies a parasitic contribution due to a deterioration of the sample surface[3], and can give rise to some ambiguities due to problems with Kramers-Krönig transformation. The more straightforward optical transmission spectra of the $LaMnO_3$ films[6] revealed a fine structure of the low-energy 2 eV band with two features near 1.7 and 2.4 eV, respectively, which were assigned in contrast with the preceding interpretations[2,3,4,5] to the Mn^{3+} d-d crystal-field transition ${}^5E_g - {}^3T_{1g}$, split by the JT effect. Such an ambiguity leaves the question of the nature of the main optical transitions in $LaMnO_3$ far from being resolved. The band structure calculations, including the LDA+U, fail to clear up the situation because of these cannot reproduce the important effects of intra-atomic correlations forming the term structure both of ground and excited CT states. In this connection a rather conventional quantum-chemical cluster approach,

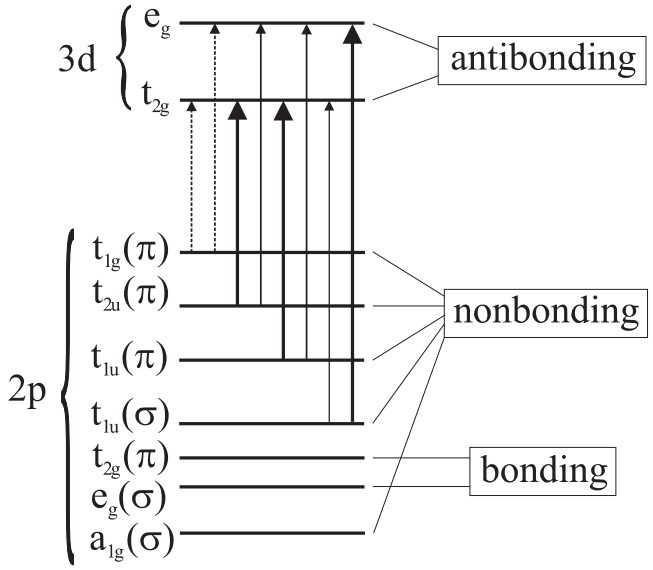

FIG. 1: The diagram of Mn 3d-O 2p molecular orbitals for the MnO_6 octahedral center. The O 2p - Mn 3d charge transfer transitions are shown by arrows: strong dipole-allowed $\sigma-\sigma$ and $\pi-\pi$ by thick solid arrows; weak dipole-allowed $\pi-\sigma$ and $\sigma-\pi$ by thin solid arrows; weak dipole-forbidden low-energy transitions by thin dashed arrows, respectively.

which combines the crystal field and the ligand field models with real opportunity to include all correlation effects, seems more relevant.

Below, in frames of such an approach we consider different CT states and O 2p-Mn 3d CT transitions in MnO_6 octahedra. As we suppose, they define the main part of the optical response both for undoped $LaMnO_3$ and different doped manganites.

II. ELECTRONIC STRUCTURE OF MANGANESE IONS AND MANGANESE-OXYGEN OCTAHEDRAL CENTERS IN MANGANITES

Five manganese Mn 3d and eighteen oxygen O 2p atomic orbitals in octahedral MnO_6 complex with the point symmetry group O_h form both hybrid Mn 3d-O 2p bonding and antibonding e_g and t_{2g} molecular orbitals (MO), and non-bonding $a_{1g}(\sigma)$, $t_{1g}(\pi)$, $t_{1u}(\sigma)$, $t_{1u}(\pi)$, $t_{2u}(\pi)$ ones.[7,8,9,10] Non-bonding $t_{1u}(\sigma)$ and $t_{1u}(\pi)$ with the same symmetry are hybridized due to the oxygen-oxygen O 2pπ - O 2pπ transfer. The relative energy position of different non-bonding oxygen orbitals is of primary importance for the spectroscopy of the oxygen-manganese charge transfer. This is firstly determined by the bare energy separation $\Delta\epsilon_{2p\pi\sigma}=\epsilon_{2p\pi}-\epsilon_{2p\sigma}$ between O 2pπ and O 2pσ electrons. Since the O 2pσ orbital points towards the two neighboring positive $3d$ ions, an electron in this orbital has its energy lowered by the Madelung potential as compared with the O 2pπ orbitals, which are perpendicular to the respective 3d-O-3d axes. Thus, Coulomb arguments favor the positive sign of the $\pi-\sigma$ separation $\epsilon_{p\pi}-\epsilon_{p\sigma}$ which numerical value can be easily estimated in frames of the well-known point charge model[7], and appears to be of the order of 1.0 eV. In a first approximation, all the $\gamma(\pi)$ states $t_{1g}(\pi), t_{1u}(\pi), t_{2u}(\pi)$ have the same energy. However, the O 2pπ-O 2pπ transfer yields the energy correction to its bare energies with the largest in value and positive in sign for the $t_{1g}(\pi)$ state. The energy of $t_{1u}(\pi)$ state drops due to hybridization with cation $4pt_{1u}(\pi)$ state. In other words, the $t_{1g}(\pi)$ state is believed to be the highest in energy non-bonding oxygen state. For illustration, in Fig.1 we show the energy spectrum of the 3d-2p manifold in octahedral complexes like MnO_6 with the relative energy position of the levels according to the X_α-method calculations[11] for the FeO_6^{9-} octahedral complex in a lattice environment typical for perovskites like $LaFeO_3$, $LaMnO_3$.

The *conventional* electronic structure of octahedral MnO_6 complexes is associated with the configuration of the completely filled O 2p shells and partly filled Mn 3d shells. The typical high-spin ground state configuration and crystalline term for Mn^{3+} in octahedral crystal field or for the octahedral MnO_6^{9-} center is $t_{2g}^3e_g^1$ and ${}^5E_g$, respectively. Namely this orbital doublet results in a vibronic coupling and Jahn-Teller (JT) effect for the MnO_6^{9-} centers, and cooperative JT ordering in $LaMnO_3$. In the framework of crystal field model the ${}^5E_g$ term originates from the $(3d^4\,{}^5D)$ term of free Mn^{3+} ion. Among the low-energy crystal field d-d transitions for the high-spin Mn^{3+} ions one should note a single spin-allowed and parity-forbidden ${}^5E_g-{}^5T_{2g}$ transition at energy varying from about 2.0 to 2.5 eV depending on the crystalline matrix. So, this is likely to be near 2.5 eV for the Mn^{3+} impurity in perovskite $YAlO_3$.[12] The transition is magneto-optically active, and could manifest itself in the Faraday and Kerr effects. A detection of the spin- and parity-forbidden ${}^5E_g-{}^3T_{1g}$ transition with, probably, lower energy could be rather important in the Mn^{3+} assignment.

The *unconventional* electronic configuration of octahedral MnO_6 complexes is associated with a *charge transfer state* with one hole in O 2p shells. The excited CT configuration $\underline{\gamma}_{2p}^1\ 3d^{n+1}$ arises from the transition of an electron from the MO predominantly anionic in nature (the γ_{2p} hole in the core of the anionic MO being hereby produced), into an empty 3d-type MO (t_{2g} or e_g). The transition between the ground configuration and the excited one can be presented as the $\gamma_{2p}\rightarrow 3d(t_{2g},e_g)$ CT transition.

The CT configuration consists of two partly filled subshells, the ligand γ_{2p}-, and the cation $3d(t_{2g}^{n_1}e_g^{n_2})$ shell, respectively. It should be emphasized that the oxygen hole having occupied the *non-bonding* γ_{2p} orbital interact *ferromagnetically* with $3d(t_{2g}^{n_1}e_g^{n_2})$ shell. This rather strong ferromagnetic coupling results in Hund rule for the CT configurations, and provides the high-spin ground states. The maximal value of the total spin for the Hund-

like CT state in MnO_6^{9-} center equals $S = 3$, that uncovers some perspectives to unconventional magnetic signatures of these states.[1]

It should be noted that the presence of the oxygen hole moving around 3d-ion in the CT state can, in common, provide a strong screening both of the 3d crystal field and intra-atomic electron-electron repulsion with the renormalization of the appropriate correlation Racah parameters A, B, C and crystal field splitting Dq. It should be noted that unlike the "monopole" parameter A the "multipole" ones B and C usually manifest relatively weak response to crystalline environment.[7] Nevertheless, all these effects can strongly complicate the calculation of the energy structure for the respective $3d^{n+1}$ configuration. This configuration in the case of CT states in MnO_6^{9-} center nominally corresponds to Mn^{2+} ion. In

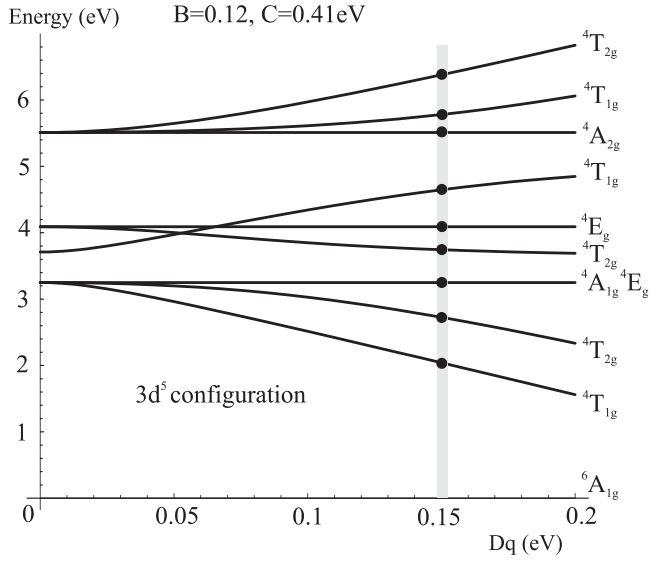

FIG. 2: The energy-level Tanabe-Sugano diagram for the high-spin terms of $3d^5$ configuration in octahedral (or cubic) crystal field.

Fig.2 we reproduce the conventional octahedral crystal field energy scheme (Tanabe-Sugano diagram) for the high-spin states of $3d^5$ configuration given the parameters $B = 0.12$, $C = 0.41$ eV typical for Mn^{2+} ions in oxides.[14,15] It is well-known that Mn^{2+} ion in cubic crystal field or the octahedral MnO_6^{10-} center manifests usually the high-spin ground state ${}^6A_{1g}$ of the $t_{2g}^3 e_g^2$ configuration. The strong Coulomb repulsion leading to the high-spin ${}^6A_{1g}$ ground term for Mn^{2+} ion would result in strong corrections to a simple picture of the energies for the CT states based on the one-electron approach sketched in Fig.1. Indeed, the one-electron model predicts the lower energy of the CT states with $3d^5; t_{2g}^4 e_g^1$ configuration rather than $3d^5; t_{2g}^3 e_g^2$ configuration. This example clearly demonstrates the role played by intra-atomic correlations. It should be noted that for the $3d^5$ configuration the ${}^6A_{1g}$ term is the only spin-sextet, so all the d-d transitions from the ground state are spin- and parity-forbidden, therefore these are extremely weak (oscillator strength $\sim 10^{-7}$)[13], and hardly observable in the optical absorption spectra. However, it has been recently shown (see Ref. 13 and references therein) that the dipole- and spin-forbidden d-d excitations can be examined excellently by spin-polarized electron energy loss spectroscopy (EELS). Fromme *et al.*[13] have measured with high accuracy ($\leq$ 0.02 eV) the excitation energies for almost all quartet ${}^4\Gamma$ terms of Mn^{2+} ions in MnO: ${}^4T_{1g}({}^4G)$ (2.13), ${}^4T_{2g}({}^4G)$ (2.4), ${}^4A_{1g}, {}^4E_g({}^4G)$ (2.82), ${}^4T_{2g}({}^4D)$ (3.31), ${}^4E_g({}^4D)$ (3.82), ${}^4T_{1g}({}^4P)$ (4.57), ${}^4A_{2g}({}^4F)$ (5.08), ${}^4T_{1g}({}^4F)$ (5.38 eV). The energy of ${}^4T_{2g}({}^4F)$ term is expected to be near 6.0 eV.[14] Simple textbook three-parameter (B, C, Dq) crystal field theory[16] provides a self-consistent description of these data given the crystal field parameter $Dq = 0.15$ eV (see Fig.2). Rigorously speaking, we should conclude $Dq = \pm 0.15$ eV because the energies of all quartet and sextet terms for the half-filled $3d^5$ configuration depend only on modulus $|Dq|$. Parameter Dq defines not only the value of the cubic crystal field splitting $\Delta = 10Dq = E(e_g) - E(t_{2g})$, but its sign. In other words, measuring only the energy of quartet terms for Mn^{2+} (or Fe^{3+}) we cannot separate two opposite cases: $E(e_g) > E(t_{2g})$ and $E(e_g) < E(t_{2g})$. However, this puzzling effect concerns only the energy rather than wave functions for the ${}^4T_g$ terms which strongly depend on the sign of Dq. Given $Dq > 0$ the lowest ${}^4T_{1g}$ term is of dominant $t_{2g}^4 e_g^1$ configuration, while for $Dq < 0$ this is of dominant $t_{2g}^2 e_g^3$ configuration. Below we shall see that the latter effect would result in very strong difference in the lineshape of the CT bands for $Dq > 0$ and $Dq < 0$ given the same energy spectrum of the CT states.

Finally, one should emphasize that both the energy and wave functions for ${}^6A_{1g}, {}^4A_{1g}, {}^4A_{2g}, {}^4E_g$ terms do not depend on the crystal field parameter Dq at all.

III. CHARGE TRANSFER TRANSITIONS IN MnO_6^{9-} CENTERS

A set of the intensive and broad absorption bands in parent manganites is usually assigned to the anion-cation O 2p-Mn 3d charge transfer.[2,3,5] In the framework of the MnO_6 center model this elementary CT process generates both intra- and inter-center CT transitions for the MnO_6^{9-} centers. The intra-center CT transitions could be associated with the *small CT Frenkel excitons*[17] and represent the oxygen hole moving around $3d^{n+1}$-cation. The inter-center CT transitions form a set of *small CT excitons*, which in terms of chemical notions represent somewhat like the *disproportionation* quanta

$$MnO_6^{9-} + MnO_6^{9-} \rightarrow MnO_6^{10-} + MnO_6^{8-} \qquad (1)$$

resulting in a formation of the bounded electron MnO_6^{10-} (e-) and hole MnO_6^{8-} (h-) small radius centers. A minimal energy of such an exciton or the disproportionation threshold usually proves to be lower than appro-

priate purely ionic quantity which value equals to the electrostatic correlation energy $U_{dd} \approx 10$ eV. The estimates made in Ref.18 yield for this energy in $LaMnO_3$: $\Delta E \approx 3.7$ eV.

A. Intra-center charge transfer transitions in MnO_6^{9-} centers

The conventional classification scheme of the CT transitions in the octahedral MnO_6^{9-} centers (intra-center CT transitions) incorporates the electric-dipole allowed transitions $\gamma_u \to 3\mathrm{d}t_{2g}, 3de_g$ from the odd oxygen $\gamma_u = t_{1u}(\pi), t_{2u}(\pi), t_{1u}(\sigma)$ orbitals to the even manganese $3\mathrm{d}t_{2g}$ and $3\mathrm{d}e_g$ orbitals, respectively. These one-electron transitions generate a manifold of the many-electron ones ${}^5E_g \to {}^5T_u$ (T_u may be equal both to T_{1u}, and T_{2u}) which may additionally differ by the crystalline term of the respective $3\mathrm{d}^{n+1}$ configuration:

$$(t_{2g}^3\,{}^4A_{2g}; e_g^1)^5E_g \to ((t_{2g}^4\,{}^3T_{1g}; e_g^1)^4\Gamma_g; \underline{\gamma_u})^5T_u, \qquad (2)$$

$$(t_{2g}^3\,{}^4A_{2g}; e_g^1)^5E_g \to ((t_{2g}^3\,{}^4A_{2g}; e_g^2; {}^{2S_1+1}\Gamma_{1g})^{2S+1}\Gamma_g; \underline{\gamma_u})^5T_u \qquad (3)$$

for $\gamma_u \to 3\mathrm{d}t_{2g}$ and $\gamma_u \to 3\mathrm{d}e_g$ transitions, respectively. Here, we already took into account the Pauli principle and the "triangle rules" for spin momenta and orbital "quasi-momenta" like Γ. Proceeding with this analysis we can obtain full selection rules for the many-electron CT transitions:

1. Each $\gamma_u \to 3\mathrm{d}t_{2g}$ transition generates two doublets of many-electron CT transitions ${}^5E_g \to {}^5T_{1,2u}$, differing by the term of the $t_{2g}^4e_g^1$ configuration: ${}^4T_{1g}$ and ${}^4T_{2g}$, respectively.

2. Each $\gamma_u \to 3\mathrm{d}e_g$ transition generates 5 many-electron CT transitions ${}^5E_g \to {}^5T_{1,2u}$, differing by the term of the $t_{2g}^3e_g^2$ configuration: ${}^4A_{1g}$, ${}^4A_{2g}$, ${}^6A_{1g}$, ${}^4E_g$, respectively (in the case of ${}^4E_g$ term each one-electron transition generates the ${}^5T_{1,2u}$ doublet). The Γ_{1g} quasi-momentum is determined by the triangle rule: $\Gamma_{1g} = A_{2g} \otimes \Gamma_g$.

Additionally, we should take into account the configurational interaction. Indeed, the terms with the same symmetry for different configurations interact and mix with each other. In our case, for the $3\mathrm{d}^5$ configuration we have 3 terms ${}^4T_{1g}$ and 3 terms ${}^4T_{2g}$ which present both in the $t_{2g}^4e_g^1$ and $t_{2g}^3e_g^2$, $t_{2g}^2e_g^3$ configurations (see Fig.2). For the $t_{2g}^3e_g^2$ configuration there are two interacting ${}^4E_g$ terms.

Hence, beginning from 3 $t_{1u}(\pi), t_{1u}(\sigma), t_{2u}(\pi)$ nonbonding purely oxygen orbitals as initial states for one-electron CT we come to 60 (!) many-electron dipole-allowed CT transitions ${}^5E_g \to {}^5T_{1,2u}$: 24 transitions $t_{1u}(\pi), t_{2u}(\pi) - t_{2g}$ ($\pi - \pi$ channel), 16 transitions $t_{1u}(\pi), t_{2u}(\pi) - e_g$ ($\pi - \sigma$ channel), 12 transitions $t_{1u}(\sigma) - t_{2g}$ ($\sigma - \pi$ channel), and 8 transitions $t_{1u}(\sigma) - e_g$ ($\sigma - \sigma$ channel), respectively. Thus, the real situation with the multi-band structure of the dipole-allowed O 2p - Mn 3d CT transitions in MnO_6^{9-} centers requires the crucial revision of the oversimplified approaches based on the concept of the only O 2p - Mn 3d CT transition[18] or at the best of two O 2p - Mn $3\mathrm{d}t_{2g}, e_g$ CT transitions.[2,3,5]

B. Dipole transition matrix elements

Making use of the Racah algebra (the method of the irreducible tensorial operators)[16,19,20] both for spins and quasimomenta we obtain after some cumbersome calculations the following expressions for the dipole transition matrix elements between the ground $(t_{2g}^3\,{}^4A_{2g}; e_g^1)^5E_g$ and excited CT states in MnO_6^{9-} octahedra:

$\gamma_u \to t_{2g}$ **transfer**

$$\langle (t_{2g}^3\,{}^4A_{2g}; e_g^1)^5E_g\mu|\hat{d}_q|((t_{2g}^4\,{}^3T_{1g}; e_g^1)^4\Gamma_g; \underline{\gamma_u})^5T_u\mu'\rangle =$$

$$(-1)^{\mu} \left\langle \begin{array}{ccc} E_g & T_{1u} & T_u \\ -\mu & q & \mu' \end{array} \right\rangle^* \langle (t_{2g}^3\,{}^4A_{2g}; e_g^1)^5E_g\|\hat{d}\|((t_{2g}^4\,{}^3T_{1g}; e_g^1)^4\Gamma_g; \underline{\gamma_u})^5T_u\rangle\,, \qquad (4)$$

where for the many-electron submatrix element

$$\langle (t_{2g}^3\,{}^4A_{2g}; e_g^1)^5E_g\|\hat{d}\|((t_{2g}^4\,{}^3T_{1g}; e_g^1)^4\Gamma_g; \underline{\gamma_u})^5T_u\rangle =$$

$$(-1)^{j(\gamma_u)}\, 3\sqrt{2}[\Gamma_g] \left\{ \begin{array}{ccc} T_2 & A_2 & T_1 \\ E & \Gamma & E \end{array} \right\} \left\{ \begin{array}{ccc} \gamma & T_1 & T_2 \\ E & \Gamma & T \end{array} \right\} \langle \gamma_u\|d\|t_{2g}\rangle \ : \qquad (5)$$

$\gamma_u \to e_g$ **transfer**

$$\langle (t_{2g}^3\,{}^4A_{2g}; e_g^1)^5E_g\mu|\hat{d}_q|((t_{2g}^3\,{}^4A_{2g}; e_g^2; {}^{2S_1+1}\Gamma_{1g})^{2S+1}\Gamma_g; \underline{\gamma_u})^5T_u\mu'\rangle =$$

$$(-1)^{\mu}\left\langle \begin{array}{ccc} E_g & T_{1u} & T_u \\ -\mu & q & \mu^{'} \end{array}\right\rangle^{*}\langle(t_{2g}^{3}\,{}^{4}A_{2g};e_g^{1})^{5}E_g\|\hat{d}\|((t_{2g}^{3}\,{}^{4}A_{2g};e_g^{2};{}^{2S_1+1}\Gamma_{1g})^{2S+1}\Gamma_g;\underline{\gamma_u})^{5}T_u\rangle\,, \tag{6}$$

where for the many-electron submatrix element

$$\langle(t_{2g}^{3}\,{}^{4}A_{2g};e_g^{1})^{5}E_g\|\hat{d}\|((t_{2g}^{3}\,{}^{4}A_{2g};e_g^{2};{}^{2S_1+1}\Gamma_{1g})^{2S+1}\Gamma_g;\underline{\gamma_u})^{5}T_u\rangle =$$

$$(-1)^{1+j(\gamma_u)+j(\Gamma)}\sqrt{6}[S_1,S,\Gamma_{1g},\Gamma_g]^{1/2}\left\{\begin{array}{ccc} 3/2 & S_1 & S \\ 1/2 & 2 & 1/2 \end{array}\right\}\left\{\begin{array}{ccc} A_2 & E & E \\ E & \Gamma & \Gamma_1 \end{array}\right\}\left\{\begin{array}{ccc} \gamma & T_1 & E \\ E & \Gamma & T \end{array}\right\}\langle\gamma_u\|d\|e_g\rangle\,. \tag{7}$$

Here, the expressions (4), (6) represent the Wigner-Eckart theorem for many-electron transition matrix elements with $\left\langle \begin{array}{ccc} \cdot & \cdot & \cdot \\ \cdot & \cdot & \cdot \end{array}\right\rangle$ being the Wigner coefficient for the cubic point group.[16,20] In (5), (7) the conventional notations are used for spin $6j$- and orbital 6Γ symbols ($\left\{ \begin{array}{ccc} \cdot & \cdot & \cdot \\ \cdot & \cdot & \cdot \end{array}\right\}$); $[S]=2S+1$, $[\Gamma]$ is the dimensionality of the corresponding irreducible representation of the cubic point group; $j(\Gamma)$ the so-called quasimomentum number; $\langle\gamma_u\|\hat{d}\|\gamma_g\rangle$ is the one-electron dipole moment submatrix element. The latter is defined by the respective Wigner-Eckart theorem as follows

$$\langle\gamma_u\mu|\hat{d}_q|\gamma_g\mu^{'}\rangle=(-1)^{j(\gamma_u)-\mu}\left\langle \begin{array}{ccc} \gamma_u & T_{1u} & \gamma_g \\ -\mu & q & \mu^{'} \end{array}\right\rangle^{*}\langle\gamma_u\|\hat{d}\|\gamma_g\rangle\,. \tag{8}$$

It should be noted that the above calculation of the dipole matrix elements implies the same character of the one-electron t_{2g},e_g orbitals both for the ground state t_{2g}^3,e_g^1 and excited $t_{2g}^3,e_g^2\;t_{2g}^4,e_g^1$ CT configurations, particularly with the invariable values of the appropriate covalency parameters.

The one-electron dipole moment submatrix elements can be rather simply evaluated in frames of the so-called "local" approximation, in which the calculation of the matrix of the dipole moment implies the full neglect all many-center integrals:

$$\langle\phi_{k_1}(\mathbf{R}_1-\mathbf{r})|\hat{\mathbf{d}}|\phi_{k_2}(\mathbf{R}_2-\mathbf{r})\rangle=e\mathbf{R}_1\delta_{\mathbf{R}_1,\mathbf{R}_2}\,\delta_{k_1,k_2}\,,$$

where $\mathbf{R}_1,\mathbf{R}_2$ label sites, k_1,k_2 atomic functions, respectively. Then

$$\langle t_{2u}(\pi)\|\hat{d}\|e_g\rangle=0;\;\langle t_{2u}(\pi)\|\hat{d}\|t_{2g}\rangle=-i\sqrt{\frac{3}{2}}\lambda_\pi d\,;$$

$$\langle t_{1u}(\sigma)\|\hat{d}\|t_{2g}\rangle=0;\;\langle t_{1u}(\sigma)\|\hat{d}\|e_g\rangle=-\frac{2}{\sqrt{3}}\lambda_\sigma d\,; \tag{9}$$

$$\langle t_{1u}(\pi)\|\hat{d}\|e_g\rangle=0;\;\langle t_{1u}(\pi)\|\hat{d}\|t_{2g}\rangle=\sqrt{\frac{3}{2}}\lambda_\pi d\,.$$

Here, $\lambda_\sigma,\lambda_\pi$ are $effective$ covalency parameters for e_g,t_{2g} electrons, respectively, $d=eR_0$ is an elementary dipole moment for the cation-anion bond length R_0. We see, that the "local" approximation results in an additional selection rule: it forbids the $\sigma\to\pi$, and $\pi\to\sigma$ transitions, $t_{1u}(\sigma)\to t_{2g}$, and $t_{1,2u}(\pi)\to e_g$, respectively, though these are dipole-allowed. In other words, in frames of this approximation only σ-type ($t_{1u}(\sigma)\to e_g$) or π-type ($t_{1,2u}(\pi)\to t_{2g}$) CT transitions are allowed. It should be emphasized that the "local" approximation, if non-zero, provides the leading contribution to transition matrix elements with corrections being of the first order in the cation-anion overlap integral. Interestingly, that the one-electron dipole moment submatrix elements for both $\pi\to\pi$ transitions in Eq. (9) have the same absolute value. Hereafter, we make use of the terminology of "strong" and "weak" transitions for the dipole-allowed CT transitions going on the $\sigma-\sigma$, $\pi-\pi$, and $\pi-\sigma$, $\sigma-\pi$ channels, respectively. Thus, for MnO_6^{9-} center we predict a series of 32 strong many-electron dipole-allowed CT transitions ${}^5E_g\to{}^5T_{1,2u}$ (24 for $\pi-\pi$, and 8 for $\sigma-\sigma$ channel) and 28 weak dipole-allowed CT transitions ($\pi-\sigma$ and $\sigma-\pi$ cross-channels).

The formulas (5)-(9) together with the numerical values of some $6j$- and 6Γ-symbols, listed below in Appendix allow to make quantitative predictions for the relative magnitude of the intensities for different CT transitions. First of all we would like to compare the overall integral intensities for the strong dipole-allowed CT transitions in the $\pi-\pi$ and $\sigma-\sigma$ channels. To this end, we calculate and sum the line strengths (the dipole submatrix element squared) which are proportional to the appropriate oscillator strengths:

$$I_{\pi\pi}=9\lambda_\pi^2\,d^2;\;I_{\sigma\sigma}=\frac{3}{2}\lambda_\sigma^2\,d^2\,, \tag{10}$$

or

$$I_{\pi\pi}/I_{\sigma\sigma}=6\lambda_\pi^2/\lambda_\sigma^2\,. \tag{11}$$

In other words, the ratio of the total oscillator strengths for these channels is determined by the ratio of the respective cation-anion charge density transfer parameters. Usually, $\lambda_\sigma^2>\lambda_\pi^2$, however, it seems the overall intensity for the $\pi-\pi$ channel can be comparable with that of for $\sigma-\sigma$ channel, or even exceed it. In frames of the separate channel we can obtain exact relations between the partial oscillator strengths for the CT transitions differing by the final state of the $t_{2g}^4e_g^1$ and $t_{2g}^3e_g^2$ configuration

for the $\pi-\pi$ and $\sigma-\sigma$ channel, respectively. For the $\pi-\pi$ channel we have

$$I(^4T_{1g};^5T_u) : I(^4T_{2g};^5T_u) = \frac{1}{2} \,:\, \frac{1}{2} \qquad (12)$$

irrespective of the type of the transferred oxygen π electron, t_{2u}, or t_{1u}. Here, each intensity represents the sum for two doublets, $^5T_{1u}$ and $^5T_{2u}$. Interestingly, the relative intensity for these two components is $3:1$ and $1:3$ for the $^4T_{1g}$ and $^4T_{2g}$ "intermediate" terms, respectively. It should be noted that absolutely the same relations are fulfilled for the weak dipole-allowed CT transitions in the $\sigma-\pi$ channel.

For the strong $\sigma-\sigma$, and weak $\pi-\sigma$ channels we have the more nontrivial relation:

$$I(^6A_{1g};^5T_u) : I(^4A_{1g};^5T_u) : I(^4E_g;^5T_u) : I(^4A_{2g};^5T_u)$$

$$= \frac{8}{15} \,:\, \frac{2}{15} \,:\, \frac{1}{9} \,:\, \frac{2}{9}\,, \qquad (13)$$

where the third transition is doublet with the equal intensity of both components. It should be reminded that all these numerical data are obtained for CT transitions to "pure" $t_{2g}^4e_g^1$ and $t_{2g}^3e_g^2$ configurations. The configuration interaction effect results in a redistribution of the respective intensities in between all interacting terms with the same symmetry.

IV. CHARGE TRANSFER TRANSITIONS IN PARENT $LaMnO_3$

Now we can apply the model theory to the undoped stoichiometric manganite $LaMnO_3$. For our analysis to be more quantitative we make two rather obvious model approximations. First of all, one assumes that for MnO_6^{9-} centers in $LaMnO_3$ as usually for cation-anion octahedra in 3d-oxides[9,10,11] the non-bonding $t_{1g}(\pi)$ oxygen orbital has the highest energy and forms the first electron removal oxygen state. Moreover, to be definite we assume that the energy spectrum of the non-bonding oxygen states for $Mn^{3+}O_6^{9-}$ centers in $LaMnO_3$ coincides with that calculated in Ref.11 for $Fe^{3+}O_6^{9-}$ in $LaFeO_3$ with the same crystalline environment, in other words, we have (in eV):

$$\Delta(t_{1g}(\pi)-t_{2u}(\pi)) \approx 0.8\,;\ \Delta(t_{1g}(\pi)-t_{1u}(\pi)) \approx 1.8\,;$$

$$\Delta(t_{1g}(\pi)-t_{1u}(\sigma)) \approx 3.0\,.$$

This is believed to be a rather reasonable choice of the energy parameters, because the purely oxygen states mainly depend only on crystalline environment. Secondly, we choose for the Racah parameters B and C the numerical values typical for Mn^{2+} in oxides, 0.12 and 0.41 eV, respectively (see above). The crystal-field parameter Dq may be varied, however, we decide in favor of only two model considerations with the same absolute value but the different sign of $|Dq| = 0.15$ eV ("conventional" $Dq>0$ and "unconventional" $Dq<0$ sign). Let us mention that this value, irrespective of the sign, provides a reasonable explanation of the Mn^{2+} spectra in MnO[13] (see above). Moreover, the photoemission data[21] are believed to confirm the relevance of this value for crystal field splitting parameter in $LaMnO_3$.

Hereafter, this set of parameters is used for the model theoretical simulation of the overall CT band in $LaMnO_3$. Firstly, we argue that the lowest in energy spectral feature observed in $LaMnO_3$ near 1.7 eV is believed to be associated with the onset of the series of the dipole-forbidden CT transitions $t_{1g}(\pi) \rightarrow e_g, t_{2g}$, rather than with any d-d crystal field transition. The energy of this transition was picked out to be a starting point to assign all other CT transitions.

Weak dipole-allowed $\pi-\sigma$ CT transitions $t_{2u}(\pi)-e_g$ and $t_{1u}(\pi)-e_g$ form more intensive CT bands starting at higher than the preceding series energies, near 2.5 and 3.5 eV, respectively, in accordance with the magnitude of the $t_{1g}(\pi)-t_{2u}(\pi)$ and $t_{1g}(\pi)-t_{1u}(\pi)$ separations. Actually, the $t_{1u}(\pi)-e_g$ transition has to be more intensive because the $t_{1u}(\pi)$ state is partly hybridized with $t_{1u}(\sigma)$, hence this transition borrows a portion of intensity from the strong dipole-allowed $t_{1u}(\sigma)-e_g$ CT transition.

The latter $\sigma-\sigma$ transition as we see from Eq.(13) forms intensive broad CT band starting from the main $^5E_g - {}^6A_{1g};{}^5T_{1u}$ peak at ≈ 4.7 eV and ranging to the $^5E_g - {}^4A_{2g};{}^5T_{2u}$ peak at ≈ 10.2 eV with interstitial peaks at ≈ 8.0 eV being the result of the superposition of two transitions $^5E_g - {}^4A_{1g};{}^5T_{1u}$ and $^5E_g - {}^4E_g;{}^5T_u$, and at ≈ 8.8 eV due to another $^5E_g - {}^4E_g;{}^5T_u$ transition, respectively. Thus, the overall width of the CT bands with final $t_{2g}^3e_g^2$ configuration occupies a spectral range from 1.7 up to ~ 10 eV.

As it is seen from Eq.(12) strong dipole-allowed $\pi-\pi$ CT transitions $t_{2u}(\pi), t_{1u}(\pi) - t_{2g}$ form two manifolds of equally intensive CT bands shifted with respect each other by the $t_{2u}(\pi)-t_{1u}(\pi)$ separation (≈ 1.0 eV). In turn, each manifold consists of two triplets of weakly split and equally intensive CT bands associated with $^5E_g - {}^4T_{1g};{}^5T_u$ and $^5E_g - {}^4T_{2g};{}^5T_u$ transitions, respectively. In accordance with the assignment of crystal-field transitions[13] in $LaMnO_3$ (see Fig.2) we should expect the low-energy edge of the dipole-allowed $\pi-\pi$ CT band starting from ≈ 4.5 eV ($1.7+2.0+(t_{1g}(\pi)-t_{2u}(\pi)$ separation)). Taking account of strong configuration interaction we should expect the high-energy edge of this band associated with the highest in energy $^4T_{2g}$ term of the $3d^5$ configuration to be situated near ≈ 9.9 eV. In between, in accordance with our scheme of energy levels we predict peaks at 5.2; 5.5; 6.2 ($\times 2$); 7.2($\times 2$); 7.9; 8.2; 8.3; 8.9 eV. The weak dipole-allowed $\sigma-\pi$ transitions occupy the high-energy spectral range from 6.7 to 11.1 eV.

Overall, our analysis shows the multi-band structure of the CT optical response in $LaMnO_3$ with the weak low-energy edge at 1.7 eV, associated with forbidden $t_{1g}(\pi)-$

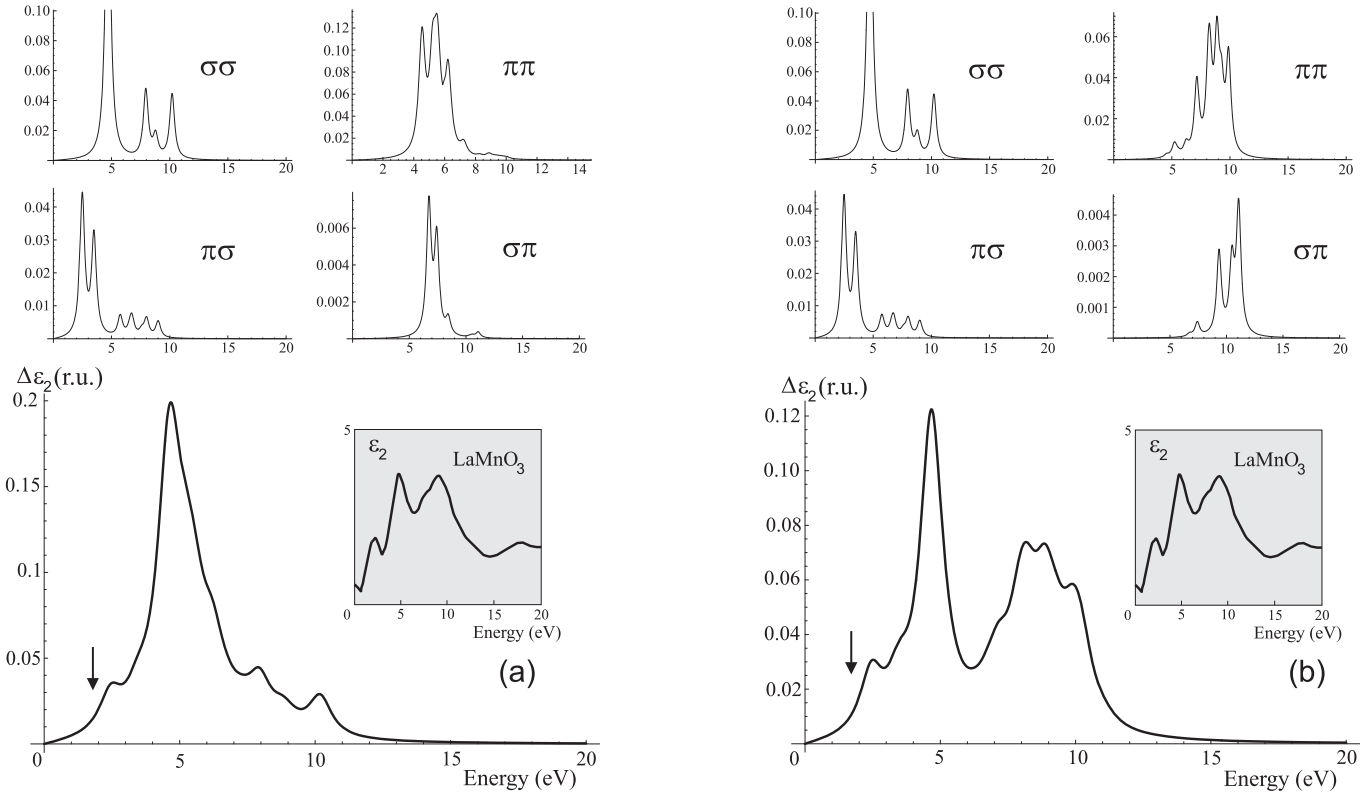

FIG. 3: Theoretical simulation of the overall O 2p-Mn 3d CT band in $LaMnO_3$ with conventional $Dq > 0$ (a) and unconventional $Dq < 0$ (b) sign for the crystal field parameter. The top panels shows the partial contributions of different dipole-allowed transitions. The lower panels present the overall contribution of the dipole-allowed CT transitions to the imaginary part of dielectric function. Experimental spectrum for $La_{1-x}Sr_xMnO_3$ given $x \approx 0$ from the paper by Okimoto *et al.*[3] is shown in insert (see text for details).

e_g transition and a series of strong bands in the range $4.6 \div 10.2$ eV beginning from composite peak at $\sim 4.5 \div 4.7$ eV and closing by composite peak at $8 \div 10$ eV both resulting from the superposition of strong dipole-allowed $\pi - \pi$ and $\sigma - \sigma$ CT transitions.

Above we addressed the model energies of the CT transitions. In frames of our model approach the relative intensities for different dipole-allowed CT transitions are governed by the relative magnitude of different one-electron dipole submatrix elements. We have performed the theoretical simulation of the overall O 2p-Mn 3d CT optical band in $LaMnO_3$ generated by dipole-allowed CT transitions in MnO_6^{9-} octahedra given simple physically reasonable assumptions concerning the one-electron submatrix elements. We have assumed: i) the equal integral intensities for the $\sigma - \sigma$ and $\pi - \pi$ channels: $I_{\sigma\sigma} = I_{\pi\pi}$, that corresponds $\lambda_\sigma^2 = 6\lambda_\pi^2$; and ii) the equal integral intensities $I_{\pi\sigma} = I_{\sigma\pi} = 0.1 I_{\sigma\sigma}$ for all weak dipole-allowed transitions $t_{2u}(\pi) - e_g$, $t_{1u}(\pi) - e_g$, and $t_{1u}(\sigma) - t_{2g}$. The former assumption agrees with the well-known semi-empirical rule that simply states: $\lambda_\sigma \sim 2\lambda_\pi$. Indeed, the theoretical calculations and experimental data for $3d^5$ configuration in FeO_6^{9-} octahedra yield: $\lambda_\sigma^2 \approx 3.5\lambda_\pi^2$ and $\lambda_\sigma^2 \approx (2.5 \div 6.0)\lambda_\pi^2$, respectively.[11,22] The latter assumption concerns the outgoing beyond the "local" approximation and seems to be more speculative. Probably, this yields an overestimation for $t_{2u}(\pi) - e_g$ transition, but underestimation for $t_{1u}(\pi) - e_g$ and $t_{1u}(\sigma) - t_{2g}$ transitions, which intensity can be enhanced due to $t_{1u}(\pi) - t_{1u}(\sigma)$ hybridization. The more detailed quantitative description of the weak dipole-allowed CT transitions needs the substantial expansion of our model approach and further theoretical studies.

The calculated model contributions of the dipole-allowed CT transitions to the imaginary part of dielectric function are presented in Figs.3a,b for conventional $Dq > 0$ (Fig.3a) and unconventional $Dq < 0$ (Fig.3b) sign for the crystal field parameter. The top panels in both cases show the partial contributions of different dipole-allowed transitions modeled by rather narrow Lorentzians with linewidth $\Gamma = 0.5$ eV to clearly reveal the multiplet structure. The lower panels present the overall contribution to the imaginary part of dielectric function of the dipole-allowed CT transitions. Here, the Lorentzian linewidth is assumed to be $\Gamma = 1.0$ eV for all contributions to maximally reproduce the experimental situation. All the spectra are presented in the same relative units.

As it was mentioned above, the energy spectrum of CT states in MnO_6^{9-} octahedra does not depend on the sign

of the crystal-field parameter Dq. However, the intensities of certain CT transitions appear to be extremely sensitive to the sign of Dq, or in other words, to the relative energy position of e_g and t_{2g} orbitals. First of all, this concerns the $\pi - \pi$ and $\sigma - \pi$ channels which manifest anomalously strong dependence on the Dq sign with clearly seen spectral weight transfer from the composite band centered around $\sim$ 5 eV given $Dq > 0$ (Fig.3a) to the composite band centered around $\sim$ 9 eV given $Dq < 0$ (Fig.3b). From the other hand, the $\sigma - \sigma$ and $\pi - \sigma$ channels which define the low-energy part of the overall CT band show no change with the Dq sign inversion. Thus, the high-energy part of the overall CT band provides a very sensitive tool to examine the screening effects for crystal field in the $3d^5$ configuration with the oxygen hole surrounding.

The theoretical findings are in reasonable quantitative agreement with experimental spectra available.[3] Indeed, a rather broad spectral structure with distinctly revealed peaks near 5 eV and $8 \div 9$ eV is observed in the ϵ_2 spectra for undoped $LaMnO_3$[3] (see inserts in Fig.3), although only the band peaked near 5 eV was assigned earlier to the O 2p-Mn 3d charge transfer. The high-energy peak at $8 \div 9$ eV was assigned by Okimoto *et al.* to O 2p-La 5d interband transitions[3] albeit this was argued rather on the quantitative considerations than either calculations. However, Arima and Tokura in their optical study of different perovskite-type RMO_3 (R=La, Y, M = Sc, Ti, V, Cr, Mn, Fe, Co, Ni, Cu)[2] have shown that similar band is commonly observed for all both $LaMO_3$ and YMO_3 compounds. In other words, it seems more natural to ascribe this band rather to the high-energy edge of the O 2p-M 3d CT transitions, than the O 2p-La 5d, O 2p-Y 4d.[2] Comparing experimental spectra[3] with simulated ones we may unambiguously assign the high-energy feature around $8 \div 9$ eV to the high-energy edge of the O 2p-Mn 3d CT transitions given the unconventional sign of the crystal field parameter $Dq < 0$ (see Fig.3b). In other words, comparing the experimentally observed relative intensities of 5 eV and $8 \div 9$ eV bands, we may conclude that the oxygen hole in the CT states of MnO_6^{9-} center can give rise to the strong overscreening of the crystal field parameter Dq resulting in the sign inversion. Generally speaking, we believe that this conclusion needs theoretical and experimental substantiation in the further studies of the CT states and transitions both in $LaMnO_3$ and another 3d oxides. Nevertheless, one should note that irrespective of the numerical value and sign of Dq, the low-energy spectral range of the overall CT band consists of a series of transitions with increasing intensity beginning from the lowest dipole-forbidden $t_{1g}(\pi) - e_g$ peaked at 1.7 eV, weakly dipole-allowed $t_{2u}(\pi) - e_g$ peaked at 2.5 eV, relatively more intensive, but weak dipole-allowed $t_{1u}(\pi) - e_g$ peaked at 3.5 eV, and, finally, strong dipole-allowed $t_{1u}(\sigma) - e_g$ transition peaked at 4.7 eV, respectively. It should be emphasized one more that the multi-band structure with a wide spectral range of the order of 10 eV represents one of the characteristic features of the O 2p - Mn 3d charge transfer optical response in $LaMnO_3$ which has to be first taken into account before any theoretical treatment of experimental spectra.

Interestingly, that with slight substitution in doped systems like $La_{1-x}Sr_xMnO_3$ the weak low-energy edge band at 1.7 eV gradually disappears[4,5] with the simultaneous shift of the high-energy bands to the lower frequencies. Our model allows to associate this effect with the localization of the doped holes in the upper purely oxygen orbitals like $t_{1g}(\pi)$, $t_{2u}(\pi)$.[1] Then the lowering of the electron density for these states would result in the lowering of the intensity for the appropriate CT bands. The red shift of the high-energy bands can result from the screening effects induced by oxygen holes mainly for the Racah parameter A.

Concluding this Section, we would like comment recent paper by N.N. Kovaleva *et al.*.[18] In frames of the fully-ionic shell model the authors explored the role of electronic and ionic polarization energies and estimated the optical CT energies. To the best of our knowledge, this is first attempt to give the realistic picture of different charge fluctuations in manganites for which the polarization energies are crucial. In what concerns the optical properties of $LaMnO_3$ the authors suggest that the band at $\sim$ 5 eV is associated with the fundamental O 2p - Mn 3d CT transition, whereas the band at $\sim$ 2 eV is rather associated with the presence of Mn^{4+} and/or O^- self-trapped holes in probably non-stoichiometric $LaMnO_3$ compound. Broad band peaked near 9 eV is assigned to O 2p - La 5d CT transition. However, their assignment is based on the numerical results obtained in frames of the semi-empirical shell model with the full neglect of the orbital degeneracy, many-electron intra-atomic correlations, and crystal field effects both for manganese and oxygen electrons. On the other hand, namely these effects are shown here to be responsible for multi-band structure of the CT optical response. In a sense, the fundamental O 2p - Mn 3d CT energy evaluated in Ref.18 to be 5.6 eV represents a mean value of the respective CT energies.

V. CONCLUSIONS

In frames of a rather conventional quantum-chemical cluster approach, which combines the crystal field and the ligand field models we have examined different CT states and O 2p-Mn 3d CT transitions in MnO_6^{9-} octahedra. The many-electron dipole transition matrix elements were calculated using the Racah algebra for the cubic point group. Simple "local" approximation allowed to calculate the relative intensity for all dipole-allowed $\pi - \pi$ and $\sigma - \sigma$ CT transitions. We present a self-consistent description of the CT bands in insulating stoichiometric $LaMnO_3$. Our analysis shows the multi-band structure of the CT optical response with the weak low-energy edge at 1.7 eV, associated with forbidden $t_{1g}(\pi) - e_g$ tran-

sition and a series of the high-energy weak and strong dipole-allowed high-energy transitions starting from 2.5 and 4.5 eV, respectively, and extending up to nearly 11 eV. The most intensive features are associated with two strong composite bands near $4.6 \div 4.7$ eV and $8 \div 9$ eV, respectively, resulting from the superposition of the dipole-allowed $\sigma - \sigma$ and $\pi - \pi$ CT transitions. These theoretical findings are in quantitative agreement with experimental spectra available. We examined the effects of the sign of the crystal field parameter Dq and showed that the $\pi - \pi$ and $\sigma - \pi$ channels contrary to $\sigma - \sigma$ and $\pi - \sigma$ ones manifest anomalously strong dependence on the Dq sign with clearly seen spectral weight transfer from the composite band centered around ~ 5 eV given $Dq > 0$ to the composite band centered around ~ 9 eV given $Dq < 0$. Thus, the high-energy part of the overall CT band provides a very sensitive tool to examine the screening effects for the crystal field in the $3d^5$ configuration with the oxygen hole surrounding. The experimental data point to a strong overscreening of the crystal-field parameter Dq in the CT states of MnO_6^{9-} centers. In addition, we would like emphasize the specific role of the intra-atomic correlation effects. It seems, the actual spectral picture of the CT optical response is determined on equal footing both by the intra-atomic d-d electron-electron repulsion and single electron effects. We believe that these and many other semi-quantitative conclusions drawn from our model will stimulate the further theoretical and experimental studies of the CT states and transitions both in $LaMnO_3$ and another 3d oxides. We did not consider the inter-center CT transitions. Its role in optical response remains so far unclear, however, appropriate intensities seem to be small because these are proportional to small inter-center d-d transfer integrals squared.

VI. ACKNOWLEDGMENTS

The discussions with N.N. Loshkareva, Yu.P. Sukhorukov, E.A. Ganshina, V.S. Vikhnin, R. Hayn, S.-L. Drechsler are acknowledged. The research described in this publication was supported in part by grant SMWK of the Ministry of Science and Art of Saxony. The author would like to thank for hospitality Institut für Festkörper- und Werkstofforschung Dresden, where part of this work was made. The author acknowledges a partial support from the Award No.REC-005 of the U.S. Civilian Research & Development Foundation for the Independent States of the Former Soviet Union (CRDF), Russian Ministry of Education, grant E00-3.4-280, and Russian Foundation for Basic Researches, grant 01-02-96404.

*

APPENDIX A: NUMERICAL VALUES FOR $6j$- AND 6Γ-COEFFICIENTS THAT ONE NEEDS TO CALCULATE THE DIPOLE TRANSITION MATRIX ELEMENTS

$$\left\{ \begin{array}{ccc} 3/2 & 1 & 5/2 \\ 1/2 & 2 & 1/2 \end{array} \right\} = -\frac{1}{\sqrt{15}}\,; \left\{ \begin{array}{ccc} 3/2 & 1 & 3/2 \\ 1/2 & 2 & 1/2 \end{array} \right\} = \frac{1}{2\sqrt{10}}\,; \left\{ \begin{array}{ccc} 3/2 & 0 & 3/2 \\ 1/2 & 2 & 1/2 \end{array} \right\} = \frac{1}{2\sqrt{2}}\,;$$

$$\left\{ \begin{array}{ccc} A_2 & E & E \\ E & A_1 & A_2 \end{array} \right\} = \left\{ \begin{array}{ccc} A_2 & E & E \\ E & A_2 & A_1 \end{array} \right\} = -\frac{1}{\sqrt{2}}\,; \left\{ \begin{array}{ccc} A_2 & E & E \\ E & E & E \end{array} \right\} = \frac{1}{2}\,;$$

$$-\left\{ \begin{array}{ccc} T_1 & T_1 & E \\ E & A_1 & T_1 \end{array} \right\} = \left\{ \begin{array}{ccc} T_1 & T_1 & E \\ E & A_2 & T_2 \end{array} \right\} = \left\{ \begin{array}{ccc} T_2 & A_2 & T_1 \\ E & T_1 & E \end{array} \right\} = \left\{ \begin{array}{ccc} T_2 & A_2 & T_1 \\ E & T_2 & E \end{array} \right\} = -\frac{1}{\sqrt{6}}\,;$$

$$\left\{ \begin{array}{ccc} T_2 & T_1 & T_2 \\ E & T_1 & T_2 \end{array} \right\} = \left\{ \begin{array}{ccc} T_1 & T_1 & T_2 \\ E & T_2 & T_1 \end{array} \right\} = -\left\{ \begin{array}{ccc} T_2 & T_1 & T_2 \\ E & T_2 & T_1 \end{array} \right\} = -\left\{ \begin{array}{ccc} T_1 & T_1 & T_2 \\ E & T_1 & T_2 \end{array} \right\} = \frac{1}{6}\,;$$

$$\left\{ \begin{array}{ccc} T_1 & T_1 & E \\ E & E & T_1 \end{array} \right\} = \left\{ \begin{array}{ccc} T_1 & T_1 & E \\ E & E & T_2 \end{array} \right\} = \left\{ \begin{array}{ccc} T_1 & T_1 & T_2 \\ E & T_2 & T_2 \end{array} \right\} =$$

$$-\left\{ \begin{array}{ccc} T_1 & T_1 & T_2 \\ E & T_1 & T_1 \end{array} \right\} = -\left\{ \begin{array}{ccc} T_2 & T_1 & T_2 \\ E & T_1 & T_1 \end{array} \right\} = -\left\{ \begin{array}{ccc} T_2 & T_1 & T_2 \\ E & T_2 & T_2 \end{array} \right\} = \frac{1}{2\sqrt{3}}\,.$$

[1] A.S. Moskvin, I.L. Avvakumov, cond-mat/0108355 (submitted to Physica B).

[2] T. Arima, Y. Tokura, J. Phys. Soc. Jap. **64**, 2488 (1995).

[3] Y. Okimoto, T. Katsufui, T. Ishikawa, A. Urushibara, T. Arima, and Y. Tokura, Phys. Rev. Lett. **75**, 109 (1995); Y. Okimoto, T. Katsufui, T. Ishikawa, T. Arima, and Y. Tokura, Phys. Rev. B **55**, 4206 (1997).

[4] J.H. Jung, K.H. Kim, T.W. Noh *et al.*, Phys. Rev. B **57**, R11043 (1998).

[5] Koshi Takenaka, Kenji Iida, Yuko Sawaki *et al.*, J. Phys. Soc. Jap. **68**, 1828 (1999).

[6] J.F. Lawler, J.G. Lunney, and J.M.D. Coey. J. Appl. Phys. Lett. **65**, 3017 (1994).

[7] I.B. Bersuker, Electronic structure and properties of transition metal compounds (introduction to the theory), New York, Wiley, 1996.

[8] B.E. Douglas, C.A. Hollingsworth, Symmetry in Bonding and Spectra, Orlando, Acad. Press, 1985.

[9] C.N.R. Rao, B. Raveau, Transition Metal Oxides, VCH, 1995.

[10] F.J. Kahn, P.S. Pershan, J.P. Remeika, Phys. Rev. **186**, 891 (1969).

[11] A.I. Liechtenstein, A.S. Moskvin, V.A. Gubanov, Fizika Tverdogo Tela **24**, 3596 (1982) (in Russian).

[12] Gen Matsumoto, J. Phys. Soc. Jap. **29**, 615 (1970).

[13] B. Fromme, U. Brunokowski, and E. Kisker, Phys. Rev. B **58**, 9783 (1998).

[14] L.E. Orgel, J. Chem. Phys. **23**, 1004 (1955); G.W. Pratt, Phys. Rev. **116**, 281 (1959).

[15] J. van Elp, R.H. Potze, H. Eskes, R. Berger, and G.A. Sawatzky, Phys. Rev. B **44**, 1530 (1991).

[16] S. Sugano, Y. Tanabe, H. Kamimura, Multiplets of Transition Metals in Crystals. N.Y.:Acad. Press., 1971; T. Inui, Y. Tanabe, Y. Onodera, Group Theory and its Application in Physics, Springer-Verlag, Berlin-Heidelberg, 1990.

[17] A.S. Davydov, Theory of Molecular Excitons, McGraw-Hill, New York, 1962.

[18] N.N. Kovaleva, J.L. Gavartin, A.L. Shluger *et al.*, cond-mat/0108207.

[19] D. A. Varshalovich, A. N. Moskalev, V. K. Khersonskii. Quantum Theory of Angular Momentum (World Scientific, Singapore, 1988).

[20] We make use of the Racah algebra for cubic point group in the form developed by Lithuanian school (see e.g. I.V. Batarunas, I.B. Levinson, Tr. AN Lit.SSR, ser. B, 2(22), Vilnius, 1960, s.15). For a rather complete summary of this approach, see e.g. A.S. Moskvin, I.G. Bostrem, Metod Neprivodimykh Tenzornykh Operatorov Tochechnykh Grup (Method of Irreducible Tensorial Operators for Point Groups), Uralskiy Universitet, Ekaterinburg, 1998, 106 s (in Russian).

[21] J.H. Park, C.T. Chen, S-.W. Cheong *et al.*, Phys. Rev. Lett. **76**, 4215 (1996).

[22] P. Freund, J. Owen, B.F. Hann, J. Phys. C: Solid St. Phys. **6**, 2139 (1973).